J Physiol 590.20 (2012) pp 5075–5090

The Journal of Physiology

A ring of threonines in the inner vestibule of the pore of CNGA1 channels constitutes a binding site for permeating ions

Arin Marchesi[1], Monica Mazzolini[1,2] and Vincent Torre[1]

[1]*Neurobiology Sector, International School for Advanced Studies (SISSA), via Bonomea, 265, 34136 Trieste, Italy*
[2]*CBM (Consorzio di Biomedicina Molecolare), Area Science Park, Basovizza 34149 Trieste, Italy*

Key points

- Cyclic nucleotide-gated (CNG) channels are multi-ion channels showing the anomalous mole fraction effect (AMFE) in the presence of Li^+ and Cs^+ mixtures.
- We show that Cs^+ ions at the intracellular side of the membrane block the entry of Na^+ ions in a voltage dependent way.
- The blockage is relieved when Thr359 and Thr360 at the intracellular entrance of the selectivity filter are replaced with an alanine. Moreover, the AMFE in the presence of intracellular mixtures of Li^+ and Cs^+ is abolished in T360A mutant channels.
- We have identified a second binding site – composed by the ring of Thr360 at the intracellular vestibule – in the selectivity filter of CNG channels controlling monovalent cations selectivity and permeation.
- These results help us understand fundamental similarities and differences between the pore of CNG channels and K^+ channels.

Abstract Cyclic nucleotide-gated (CNG) channels and K^+ channels have a significant sequence identity and are thought to share a similar 3D structure. K^+ channels can accommodate simultaneously two or three permeating ions inside their pore and therefore are referred to as multi-ion channels. Also CNGA1 channels are multi-ion channels, as they exhibit an anomalous mole fraction effect (AMFE) in the presence of mixtures of 110 mM Li^+ and Cs^+ on the cytoplasmic side of the membrane. Several observations have identified the ring of Glu363 in the outer vestibule of the pore as one of the binding sites within the pore of CNGA1 channels. In the present work we identify a second binding site in the selectivity filter of CNGA1 channels controlling AMFE. Here, we show also that Cs^+ ions at the intracellular side of the membrane block the entry of Na^+ ions. This blockage is almost completely removed at high hyperpolarized voltages as expected if the Cs^+ blocking site is located within the transmembrane electric field. Indeed, mutagenesis experiments show that the block is relieved when Thr359 and Thr360 at the intracellular entrance of the selectivity filter are replaced with an alanine. In T359A mutant channels AMFE in the presence of intracellular mixtures of Li^+ and Cs^+ is still present but is abolished in T360A mutant channels. These results suggest that the ring of Thr360 at the intracellular entrance of the selectivity filter forms another ion binding site in the CNGA1 channel. The two binding sites composed of the rings of Glu363 and Thr360 are not independent; in fact they mediate a powerful coupling between permeation and gating, a specific aspect of CNG channels.

DOI: 10.1113/jphysiol.2012.238352

(Received 6 June 2012; accepted after revision 3 August 2012; first published online 6 August 2012)
Corresponding author V. Torre: Neurobiology Sector, International School for Advanced Studies (SISSA), via Bonomea, 265, 34136 Trieste, Italy. Email: torre@sissa.it

Abbreviations AMFE, anomalous mole fraction effect; CNG channel, cyclic nucleotide-gated channel; DMA, dimethylammonium; i_{sc}, single channel current; MA, methylammonium; MD, molecular dynamics; P_o, open probability; V_{rev}, reversal potential.

Introduction

Cyclic nucleotide-gated (CNG) channels play an essential role in visual and olfactory transduction, where they are part of the biochemical machinery amplifying and translating sensory signals into neuronal activity (Stryer, 1986; Menini, 1995; Kaupp & Seifert, 2002; Craven & Zagotta, 2006; Biel & Michalakis, 2009). In rod photoreceptors CNG channels open in dark conditions and a steady inward current – referred to as the dark current – flows through them keeping photoreceptor membrane depolarized. CNG channels have also been found in the kidney, testis and brain, where their functions have not been fully understood (Zufall *et al.* 1997; Kaupp & Seifert, 2002; Togashi *et al.* 2008; Lopez-Jimenez *et al.* 2012). In vertebrates, seven members of the CNG channel gene family have been identified (Kaupp & Seifert, 2002; Tetreault *et al.* 2006; Biel & Michalakis, 2009). According to sequence similarity these genes are grouped into two subtypes, CNGA (CNGA1–CNGA5) and CNGB (CNGB1 and CNGB3). CNGA1, CNGA2, CNGA3 and CNGA5 (but not CNGA4), can form cyclic nucleotide-activated homomeric channels, while CNGB1 and CNGB3 are modulatory subunits that cannot form functional homomeric channels (Kaupp & Seifert, 2002; Craven & Zagotta, 2006; Tetreault *et al.* 2006; Biel & Michalakis, 2009). CNG channels and K^+ channels share the same transmembrane gross topology and are believed to have evolved from a common ancestor (Jan & Jan, 1990, 1992; Hille, 1992; Yu *et al.* 2005), but CNG channels are only slightly voltage dependent and, for opening, require the binding of cGMP or cAMP to a binding site located in their C-terminal portion (Stryer, 1986; Zimmerman, 1995; Biel *et al.* 1999; Kaupp & Seifert, 2002; Craven & Zagotta, 2006, Mazzolini *et al.* 2010). Cation-permeation and gating properties of homomeric recombinant and native channels are similar but not identical (Kaupp *et al.* 1989; Menini, 1990; Nizzari *et al.* 1993; Kaupp & Seifert, 2002). CNGA1 and K^+ channels have a significant amino acid identity in the pore region (23%) and presumably share the same molecular architecture (Becchetti *et al.* 1999; Flynn & Zagotta, 2001; Anselmi *et al.* 2007; Mazzolini *et al.* 2010). However, CNG and K^+ channels have different functional and structural properties: in voltage gated K^+ channels (K_v), the gating mechanism consists in the closure of the intracellular gate associated to a large bending of the S6 helices. In CNG channels, a similar bending of the S6 helices occurs (Flynn & Zagotta, 2001, 2003; Nair *et al.* 2009) but does not act as the primary gate of CNG channels, which has been located in the selectivity filter (Fodor *et al.* 1997; Becchetti *et al.* 1999; Becchetti & Roncaglia, 2000; Liu & Siegelbaum, 2000; Giorgetti *et al.* 2005; Contreras & Holmgren, 2006; Contreras *et al.* 2008; Mazzolini *et al.* 2009).

CNG channels are poorly selective and are permeable to all alkali monovalent cations (Li^+, Na^+, K^+, Rb^+ and Cs^+), while K^+ channels are permeable only to K^+ and Rb^+ (Kaupp *et al.* 1989; Menini, 1990; Hille, 1992). K^+ channels can accommodate at the same time several permeating ions inside their pore in a single file and are referred to as multi-ion channels (Hille, 1992). This fundamental property was originally inferred from electrophysiological and radioactive tracer experiments (Hodgkin & Keynes, 1955; Hille & Schwarz, 1978) and was confirmed by direct structural data of the crystal structure of K^+ channels (Doyle *et al.* 1998). The widely accepted view of permeation across K^+ channels follows Hodgkin and Keynes's knock-on model, in which conduction is driven by an incoming ion that 'knocks on' ion(s) and water molecule(s) in a concerted way. A standard way to establish the multi-ion nature of an ion channel is to verify the existence of the anomalous mole fraction effect (AMFE). The presence of the AMFE can be established by analysing the current carried by mixtures of two permeating ions X^+ and Y^+ while holding their total concentrations ($[X^+]+[Y^+]$) constant (Hagiwara *et al.* 1977; Hille & Schwarz, 1978). If the current or reversal potential V_{rev} does not change monotonically with the mole fraction $[X^+]/([X^+]+[Y^+])$ of X^+, this 'anomaly' is assumed to signal the multi-ion nature of the channel (Hille & Schwarz, 1978). Also CNG channels are multi-ion channels: in the presence of mixtures of 110 mM Li^+ and Cs^+ on the cytoplasmic side of the membrane, AMFE was observed both in native CNG channels from salamander rods and in recombinant WT CNGA1 channels from bovine rods (Sesti *et al.* 1995). AMFE was not observed in the channel where glutamate 363 (Glu363) in the pore region was mutated to a glutamine (E363Q) or an asparagine (E363N). These results and similar electrophysiological observations (Furman & Tanaka, 1990; Qu *et al.* 2001) have identified the ring of Glu363 as forming one binding site within the pore of CNGA1 channels (Root & MacKinnon, 1993, 1994; Eismann *et al.* 1994; Rho & Park,

1998) but the other binding sites have not been identified and have remained elusive even after two decades from the original cloning of CNGA1 channels.

A variety of K^+ channels have been crystallized (Doyle *et al.* 1998; Jiang *et al.* 2002, 2003; Long *et al.* 2005; Tao *et al.* 2009; Brohawn *et al.* 2012) and their molecular structure has been solved at an atomic resolution. In contrast, the molecular structure of CNG channels has not been solved at an atomic scale (Higgins *et al.* 2002) and can be inferred by combining homology modelling and electrophysiological data (Giorgetti *et al.* 2005; Mazzolini *et al.* 2010). By replacing the pore of the NaK channel with the pore of CNG (Derebe *et al.* 2011*b*), the molecular structure of a good mimic has been obtained at atomic resolution providing a framework for rationalizing a multitude of the electrophysiological data obtained so far. In the present paper we show that the ring of Thr360 at the intracellular vestibule of CNGA1 channels forms another binding site inside the pore. Our electrophysiological observations and the molecular structure of the pore of the CNG mimics (Derebe *et al.* 2011*b*) clarify the molecular mechanisms controlling ionic permeation through CNG channels and pinpoint similarities and differences with K^+ channels.

Methods

Ethical approval

All the studies have been approved by the SISSA's Ethics Committee according to the Italian and European guidelines for animal care (d.l. 116/92; 86/609/C.E.).

Molecular biology

The CNGA1 channel from bovine rod consisting of 690 amino acids was used. Selected residues were replaced as previously described (Becchetti *et al.* 1999) using the Quick Change Site-Directed Mutagenesis kit (Stratagene). Point mutations were confirmed by sequencing. cDNAs were linearized and were transcribed to cRNA *in vitro* using the mMessagemMachine kit (Ambion, Austin, TX, USA).

Oocyte preparation and chemicals

Mutant channel cRNAs were injected into *Xenopus laevis* oocytes ('Xenopus express' AncienneEcole de Vernassal, Le Bourg 43270, Vernassal, Haute-Loire, France). Oocytes were prepared as previously described (Nizzari *et al.* 1993). Injected eggs were maintained at 18°C in a Barth solution supplemented with 50 μg ml^{-1} of gentamycin sulfate and containing (in mM): 88 NaCl, 1 KCl, 0.82 $MgSO_4$, 0.33 $Ca(NO_3)_2$, 0.41 $CaCl_2$, 2.4 $NaHCO_3$, 5 Tris-HCl, pH 7.4 (buffered with NaOH). During the experiments, oocytes were kept in a Ringer solution containing (in mM): 110 NaCl, 2.5 KCl, 1 $CaCl_2$, 1.6 $MgCl_2$, 10 Hepes-NaOH, pH 7.4 (buffered with NaOH). Usual salts and reagents were purchased from Sigma-Aldrich Co. (St Louis, MO, USA).

Recording apparatus and solutions

cGMP-gated currents from excised patches were recorded with a patch-clamp amplifier (Axopatch 200, Axon Instruments Inc., Union City, CA, USA), 2–6 days after RNA injection, at room temperature (20–24°C). The perfusion system was as described (Sesti *et al.* 1995) and allowed a complete solution change in less than 1 s. Borosilicate glass electrode resistance was about 4–5 MΩ and 1–2 MΩ in symmetrical standard solution for single channel and macroscopic current recordings, respectively. The standard solution on both sides of the membrane consisted of (in mM): 110 NaCl, 10 Hepes and 0.2 EDTA (pH 7.4). In AMFE experiments, intracellular NaCl was replaced by an equimolar amount of the indicated Li^+ and Cs^+ mixtures ([LiCl] + [CsCl] = 110 mM). Traces were low-pass filtered at 2 kHz and sampled at 10 kHz. Clampex 10.0, Clampfit 10.1, and SigmaPlot 9.0 were used for data acquisition and analysis. Data are shown as mean ± SEM. *n* represents the number of patches.

Data analysis

Open probability (P_o) and single channel currents (i_{sc}) were estimated from patches containing only one CNGA1 channel fitting normalized all-point histograms with two component Gaussian functions as previously described (Bucossi *et al.* 1997). Open and closed dwell-time histograms were obtained using the pCLAMP 10 software for 50% threshold crossing analysis. Time constants (τ) were obtained from fitting open and shut times histograms with one or two exponential functions (Nizzari *et al.* 1993). Permeability ratios relative to Na^+ P_X/P_{Na} were computed from the reversal potential V_{rev} as previously described (Gamel & Torre, 2000).

Molecular modelling

Sequence alignments were based on published data. Pore cartoons were prepared using known structures of K_v and NaK chimeric channels available in the Protein Data Bank (PDB) using the DeepView module of the Swiss-PDBViewer (v4.04) software (Guex & Peitsch, 1997).

Results

Sequence alignment of the pore region of tetrameric cation channels has identified basic differences between K^+ and

CNG channels (Heginbotham *et al.* 1992; Gamel & Torre, 2000; Kaupp & Seifert, 2002; Zagotta, 2006). The pore of K^+ channels has the well known signature TXGXG (where X denotes an hydrophobic amino acid) present in all known K^+ channels either voltage gated or not. In contrast, CNG channels do not have in their pore the sequence GXG, but contain an ETPP motif flanking the conserved TXG residues (Fig. 1*A*) at their C-terminal side. These amino acid differences are expected to be at the basis of the different selectivity and permeation of K^+ and CNG channels (Heginbotham *et al.* 1992, 1994; Zagotta, 2006).

In the high-resolution structures of all K^+ channels, from bacteria to mammals (Zhou *et al.* 2001; Jiang *et al.* 2003; Long *et al.* 2005; Tao *et al.* 2009; Ye *et al.* 2010; Brohawn *et al.* 2012), the selectivity filter contains four contiguous and chemically similar ion-binding sites, termed S_1–S_4, numbered progressively from the extracellular to the intracellular side (Fig. 1*B*). The three outermost sites (S_1–S_3) are formed by carbonyl oxygen atoms whereas site S_4 is formed by four carbonyl oxygen atoms and four hydroxyl group of threonines (Fig. 1*B*).

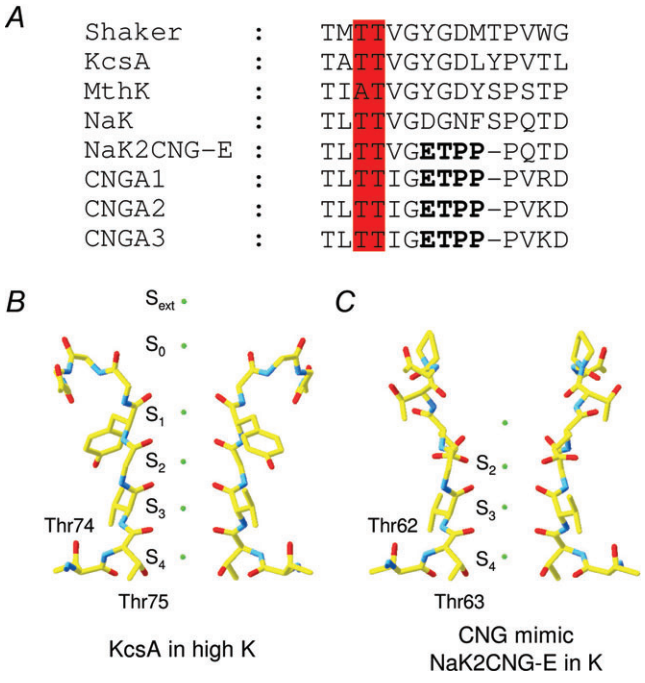

Figure 1. Partial sequence alignment among different ion channels and molecular structure of the KcsA and CNG mimicking NaK chimera
A, sequence alignment of the selectivity filter of K^+ channels (Shaker, KcsA and MthK), NaK, CNG mimicking NaK chimera (NaK2CNG-E) and the bovine subunits CNGA1-CNGA3. The ETPP motif in the CNG signature is marked in bold; conserved threonines are highlighted in red. *B*, partial molecular structure of the KcsA crystal structure as deposited in the Protein Data Bank (PDB entry code 1K4C) featuring the selectivity filter in two diagonally opposite subunits. *C*, the same as in *B* but for the NaK mimicking CNG channel obtained from the NaK2CNG-E crystal structure (PDB entry code 3K0D).

K^+ ions bind at the centre of these sites surrounded by eight oxygen ligands in a square antiprism configuration. Two additional binding sites were also located on the extracellular side of the channel (S_0 and S_{ext}). It is believed that ion conduction involves transitions between states with two and three K^+ ions occupying the selectivity filter, where ion-channel attraction and ion–ion repulsion underlie the high K^+ turnover rates (Bernèche & Roux, 2001, 2003; Morais-Cabral *et al.* 2001).

At present, the crystal structure of CNG channels has not yet been solved, but mimics of their filter region are available. Indeed, a set of chimeric NaK channels mimicking CNG channels – generated by replacing the NaK selectivity filter sequence with those of CNG – have been constructed and their crystal structure solved (Derebe *et al.* 2011*b*). The selectivity filter of NaK2CNG-E chimera adopts an architecture intermediate between that of NaK and KcsA pores and contains only three contiguous ion binding sites equivalent to sites S_2–S_4 of the KcsA (Fig. 1*C*). The S_1 site in these chimeras is replaced by a concave funnel shaped vestibule where water molecules participate in stabilizing cations entering or exiting the filter (Fig. 1*C*). Similarly to K^+ channels, these mimics have an intracellular vestibule composed of conserved threonines, which in CNGA1 channels from bovine rods are Thr359 and Thr360.

While the role in ion conduction, permeation and blockage of Glu363 in CNGA1 channels has been extensively investigated (Root & MacKinnon, 1993, 1994; Eismann *et al.* 1994; Sesti *et al.* 1995; Rho & Park, 1998), little is known about the role of Thr360 and Thr359 at the intracellular mouth. In the crystal structure of the NaK2CNG-E chimera, the last ion binding site (S_4) is formed by the side chains of Thr63 and the carbonyl oxygen of Val64, equivalent to residues Thr360 and Ile361 in CNGA1 (Fig. 1*A* and *C*), while Thr62, equivalent to residue Thr359, is buried underneath the external surface of the protein.

Intracellular Rb^+ and Cs^+ affect inward Na^+ current in WT CNGA1

In order to investigate the role of Thr359 and Thr360, we expressed WT and mutant CNGA1 channels in *Xenopus* oocytes and we recorded ionic currents evoked by 1 mM cGMP added to the intracellular side of excised patches under voltage clamp conditions (Hamill *et al.* 1981). The current flowing through CNGA1 channels was obtained as the difference of the current measured in the presence of 1 mM cGMP and in its absence.

We have analysed the blocking effect of the monovalent alkali cation X^+ (where X^+ could be Li^+, Na^+, K^+, Rb^+ or Cs^+) on the inward current carried by Na^+ ions (I_X). In these experiments the patch pipette was

filled with 110 mM NaCl and we tested the effect of a similar amount of LiCl, NaCl, KCl, RbCl and CsCl perfused in the medium bathing the intracellular side of the membrane patch (Fig. 2*A*). We stepped the voltage from a holding potential of 0 mV from –100 to +40 mV in steps of 20 mV. At negative voltages, such as −100 mV, I_X is almost unaffected by the presence of Li^+, and K^+ at the intracellular side of the membrane (Fig. 2*B* and online Supplemental Material, Supplementary Fig. 1). In contrast, I_X is smaller in the presence of Rb^+ and even more so in the presence of Cs^+ (Fig. 2*B*). The *I–V* relationships and Na^+ fractional inward current in the presence of the ionic species X in the bathing medium (I_X/I_{Na}) are shown in Fig 2*C* and *D*. In the presence of intracellular Rb^+ or Cs^+ sodium current inhibition is almost completely removed at voltages more negative than −100 mV (Fig. 2*D* and Supplementary Fig. 2). Therefore this blockage is voltage dependent, as expected when the Cs^+ blocking site is located within the transmembrane electric field.

In order to understand the molecular mechanisms of Cs^+ blockage, we analysed the effect of Cs^+ ions at the single channel level. In the presence of Na^+ ions at both sides of the membrane, the single channel current (i_{sc}) was -2.2 ± 0.3 pA and the open probability (P_o) was 0.71 ± 0.04 ($n = 6$; Fig. 3*A* and *B*) in agreement with previous reports (Nizzari *et al.* 1993). At −100 mV the mean open and closed times were 1.1 ± 0.1 and 0.7 ± 0.1 ms, respectively (Fig. 3*C*). When Na^+ bathing the intracellular side of the membrane patch was replaced by Cs^+, channel openings became smaller and less frequent (Fig. 3*D*). The analysis of the current amplitude histograms indicated

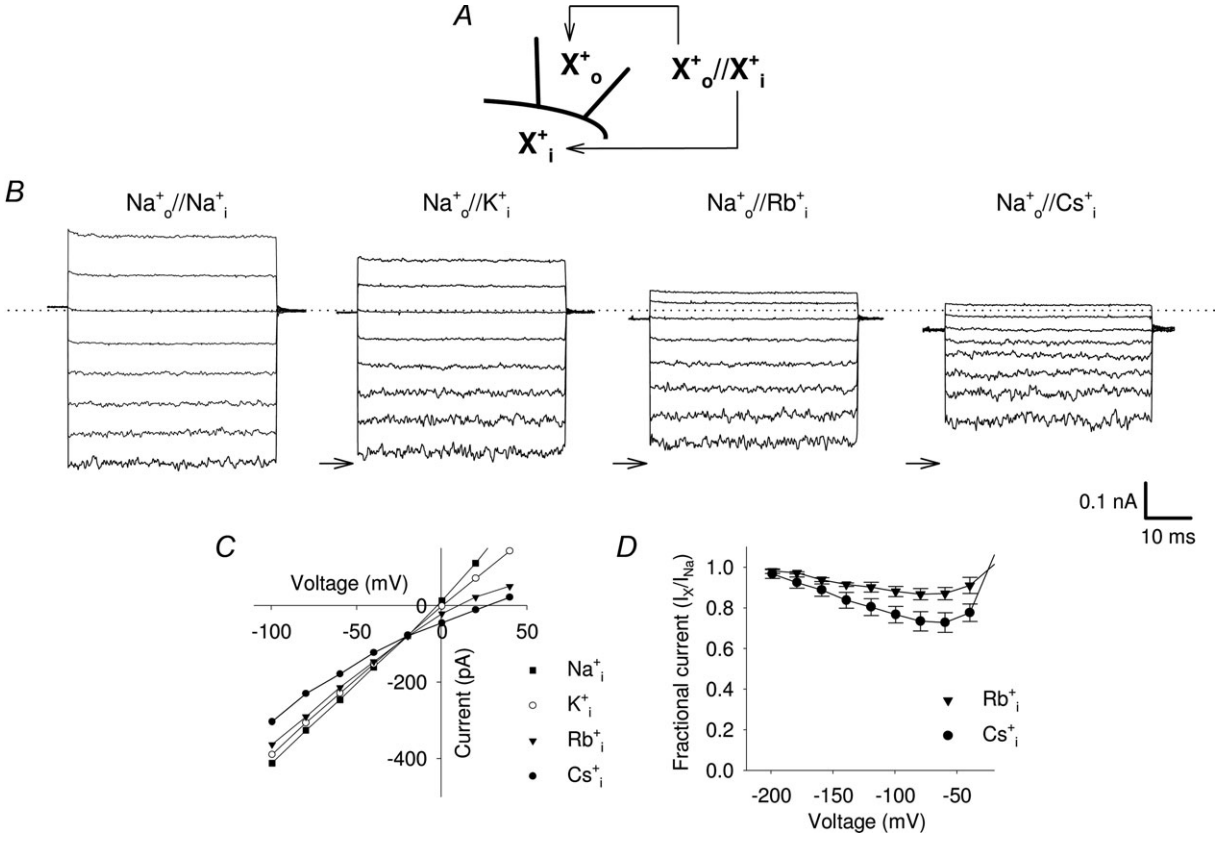

Figure 2. Voltage-dependent blockage of Na^+ current by intracellular Rb^+ and Cs^+ ions in WT CNGA1 channels

A, scheme illustrating the nomenclature used for designating intracellular (X_i^+) and extracellular (X_o^+) solutions. X^+ is the indicated monovalent cation. *B*, representative WT CNGA1 current recordings from one excised-patch in Na^+ symmetrical conditions (110 mM Na_o^+/110 mM Na_i^+) and when intracellular Na^+ was replaced by an equimolar amount of K^+, Rb^+ and Cs^+, respectively (110 mM Na_o^+/110 mM K_i^+, 110 mM Na_o^+/110 mM Rb_i^+ and 110 mM Na_o^+/110 mM Cs_i^+). Currents were elicited in the presence of 1 mM cGMP in the bathing medium and voltage steps ranging from −100 to 40 mV (ΔV = 20 mV). Dashed line indicates 0 current level; arrows indicate the −100 mV Na^+ current level in symmetrical solution. *C*, *I–V* curves in WT CNGA1 channels in the presence of 110 mM intracellular Na^+ (filled squares), K^+ (open circles), Rb^+ (filled triangles) and Cs^+ (filled circles). *D*, dependency of residual fractional Na^+ current I_X/I_{Na} on voltage when Rb^+ (filled triangles; n = 5) and Cs^+ ions (filled circles; n = 6) are in the bathing medium.

that i_{sc} decreased to about -1.7 ± 0.2 pA and P_o reduced to 0.51 ± 0.05 ($n = 5$; Fig. 3*E*). At the same time, longer closures were observed: indeed, in the presence of Cs^+ ions, the distribution of closure times was fitted by the sum of two exponential distributions with a mean closure time of 0.5 ± 0.1 and 3.8 ± 0.2 ms (Fig. 3*F*). Therefore the blockage of I_X observed in Fig. 2 caused by Cs^+ ions is produced by the combination of a reduced single channel conductance and the appearance of longer closure times.

Thr359 and Thr360 control Rb^+, Cs^+ and ammonium derivatives blockage

Previous analyses have established that the stretch of amino acids from Thr359 to Gly362 form the intracellular mouth of the pore of CNGA1 channels (Becchetti *et al.* 1999; Becchetti & Roncaglia, 2000) in agreement with the recently determined structure of the pore of CNG mimics (Fig. 1*C*). Therefore Thr359 and Thr360 are good candidates to form the intracellular binding site for Cs^+. We analysed the blockage of I_X by Rb^+ and Cs^+ ions in mutant channels T359A (Fig. 4*A* and *C*) and T360A (Fig. 4*B* and *D*). As shown in Fig. 4*E*, in this case Rb^+ inhibition of Na^+ current is abolished in both mutant channels. In T359A mutant channel Cs^+ inhibition is significantly reduced and the Na^+ fractional current (I_{Cs}/I_{Na}) becomes equal to 0.92 ± 0.02 at -100 mV (Fig. 4*F*; $n = 6$). In mutant channels T360A, I_X is almost the same in the presence of Na^+, Rb^+ or Cs^+ ions at all voltages between -40 mV and -200 mV (Fig. 4*E* and *F*).

Previous investigations (Picco & Menini, 1993) have shown that in native CNG channels Na^+ inward current is reduced by the presence of intracellular ammonium derivatives, suggesting that organic cations occupy a weakly voltage-dependent binding site in the intracellular vestibule. Therefore we investigated the effect

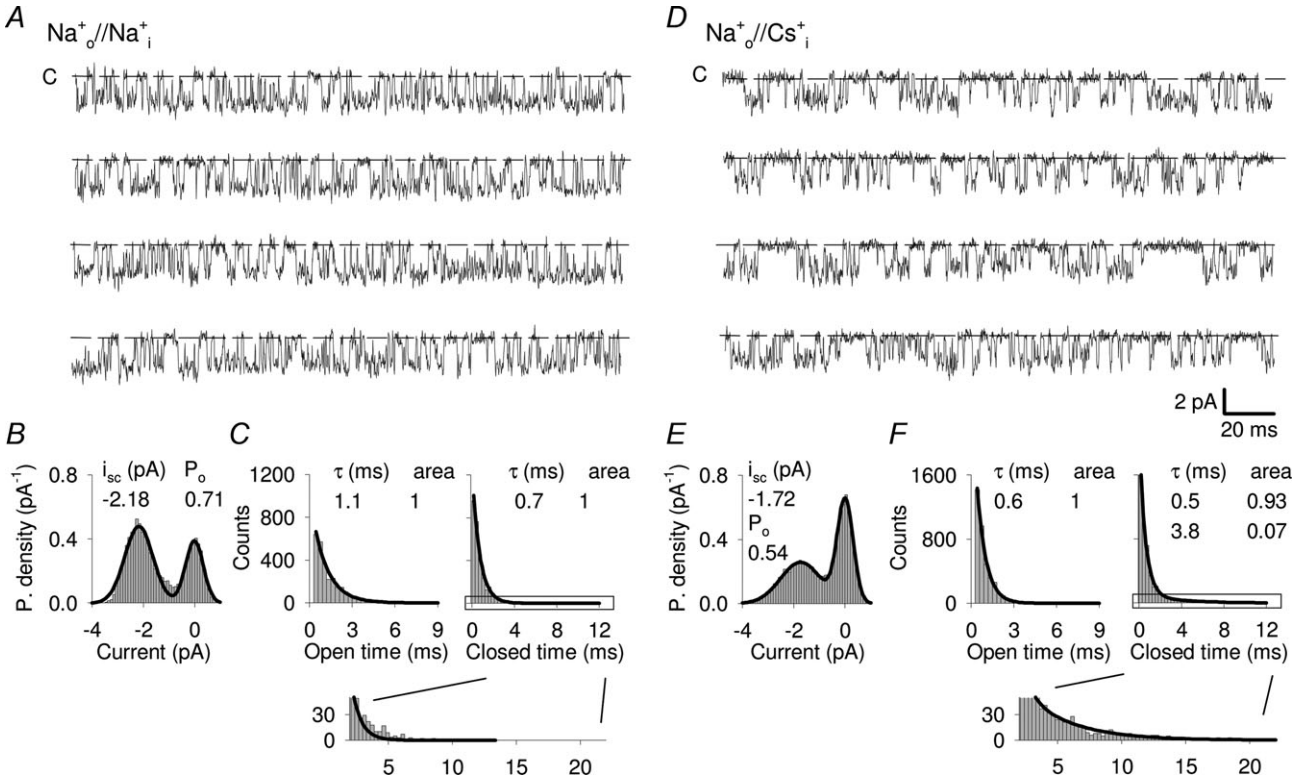

Figure 3. Single channel recordings of inward Na^+ current in the presence of intracellular Na^+ and Cs^+
A, current recording from a single WT CNGA1 channel at -100 mV in the presence of 1 mM cGMP in symmetrical Na^+. Dashed line indicates the closed state. *B*, all-point amplitude histograms from recordings as in *A*. The continuous line represents a two-component Gaussian fit. i_{sc} and P_o indicate the single channel current and the open probability. *C*, open (left panel) and closed (right panel) dwell-time distribution histograms from recordings as in *A*. The continuous line represents a one-component exponential fit. τ indicates the time constant. Inset shows an enlargement of closed dwell-time distribution. *D*, as in *A*, but when Na^+ ions in the bathing medium were replaced by Cs^+. *E* and *F*, as in *B* and *C*, respectively, but from recordings where bathing Na^+ ions were replaced with Cs^+. The continuous line in the closed dwell-time distribution (right panel) represents a two-component exponential fit. Open and closed dwell-time distribution histograms were obtained from at least 10 s recordings.

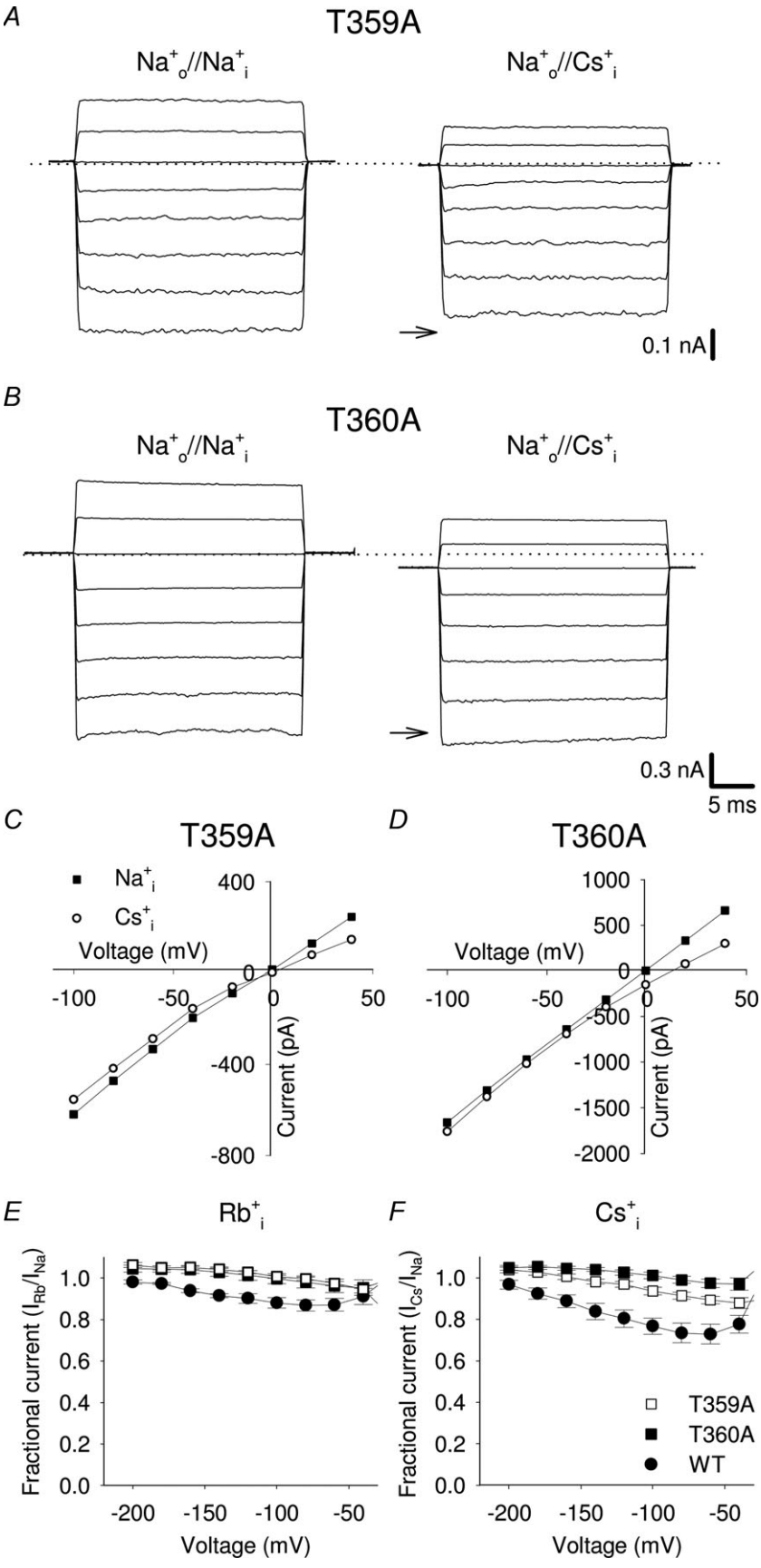

Figure 4. Voltage-dependent blockage of inward Na^+ current by intracellular Rb^+ and Cs^+ ions in T359A and T360A mutant channels
A, T359A current recordings from excised-patch in Na^+ symmetrical conditions and when intracellular Na^+ was replaced by an equimolar amount of Cs^+. Recording conditions as described in Fig. 2. Dashed line indicates 0 current level; arrows indicate the −100 mV Na^+ current level in symmetrical conditions. *B*, as in *A*, but for T360A mutant channel. *C*, *I–V* curves in T359A mutant channels in the presence of 110 mM intracellular Na^+ (filled squares), and Cs^+ (open circles). *D*, as in *C*, but for T360A mutant channel. *E*, dependency of I_{Rb}/I_{Na} on voltage for WT (filled circles), T359A (open squares) and T360A (filled squares), respectively ($n \geq 5$). *F*, as in *E*, but when intracellular Rb^+ ions were replaced with Cs^+ ($n \geq 6$).

of 110 mM intracellular methylammonium (MA) and dimethylammonium (DMA) on I_X in WT CNGA1 and T360A mutant channels. I_X is inhibited when MA or DMA ions are present in the intracellular solution (Fig. 5*A* and *C*), being Na^+ fractional current (I_X/I_{Na}) at –100 mV equal to 0.85 ± 0.03 ($n = 5$) and 0.76 ± 0.02 ($n = 6$), respectively (Fig. 5*E*). The Na^+ current blockage is larger in the presence of DMA with a weak voltage dependency (Fig. 5*E*). MA and DMA blockage of I_X is abolished in mutant channel T360A (Fig. 5*B*, *D* and *E*). Na^+ currents at –100 mV in the presence of MA and DMA are larger than those in the presence of Na^+, because when Na^+ is replaced by MA or DMA the reversal potential shifts from 0 mV up to 60 mV, so that the driving force for Na^+ influx at −100 mV in the presence of these cations is larger than in symmetrical Na^+. These results support the notion that the ring of Thr360 forms a binding site for Cs^+ as well as for methylated ammonium cations.

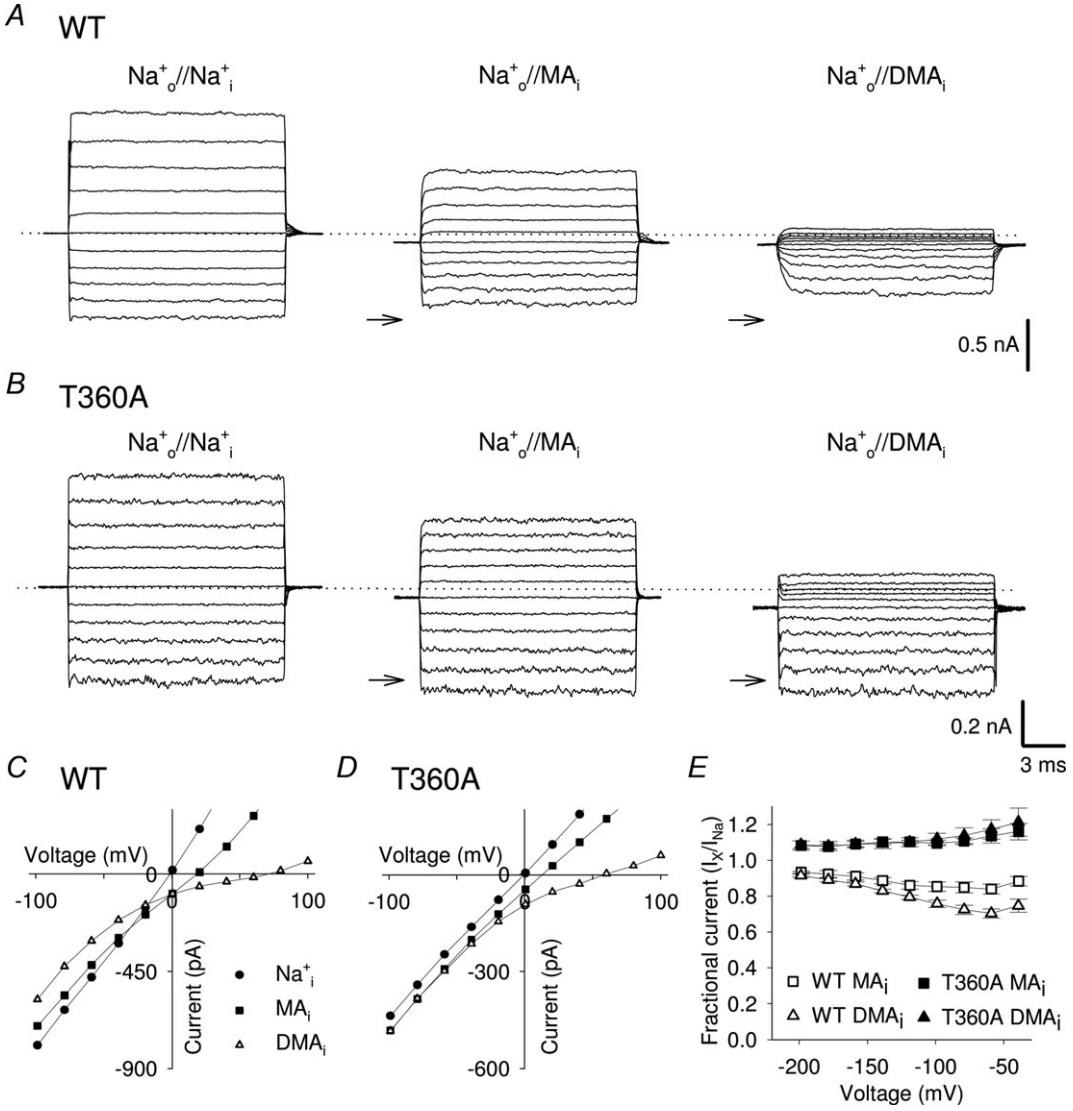

Figure 5. Voltage-dependent blockage of the of inward Na^+ current by intracellular organic cations in WT and T360A mutant channels

A, representative macroscopic WT current recordings from one excised patch in Na^+ symmetrical conditions and when intracellular Na^+ was replaced by an equimolar amount of MA and DMA. Currents were elicited in the presence of 1 mM cGMP in the bathing medium and voltage steps ranging from −100 to +100 mV (ΔV = 20 mV). Dashed line indicates 0 current level; arrows indicate the −100 mV Na^+ current level in symmetrical solution. *B*, as in *A*, but for T360A mutant channel. *C*, *I–V* curves in WT channels in the presence of 110 mM intracellular Na^+ (filled circles), MA (filled squares) and DMA (open triangles). *D*, as in C, but for T360A mutant channel. *E*, dependency of I_X/I_{Na} on voltage when MA ions (open and filled squares) and DMA ions (open and filled triangles) were in the bathing medium for WT (open symbols; $n \geq 5$), and T360A (filled symbols; $n = 4$) mutant channel, respectively.

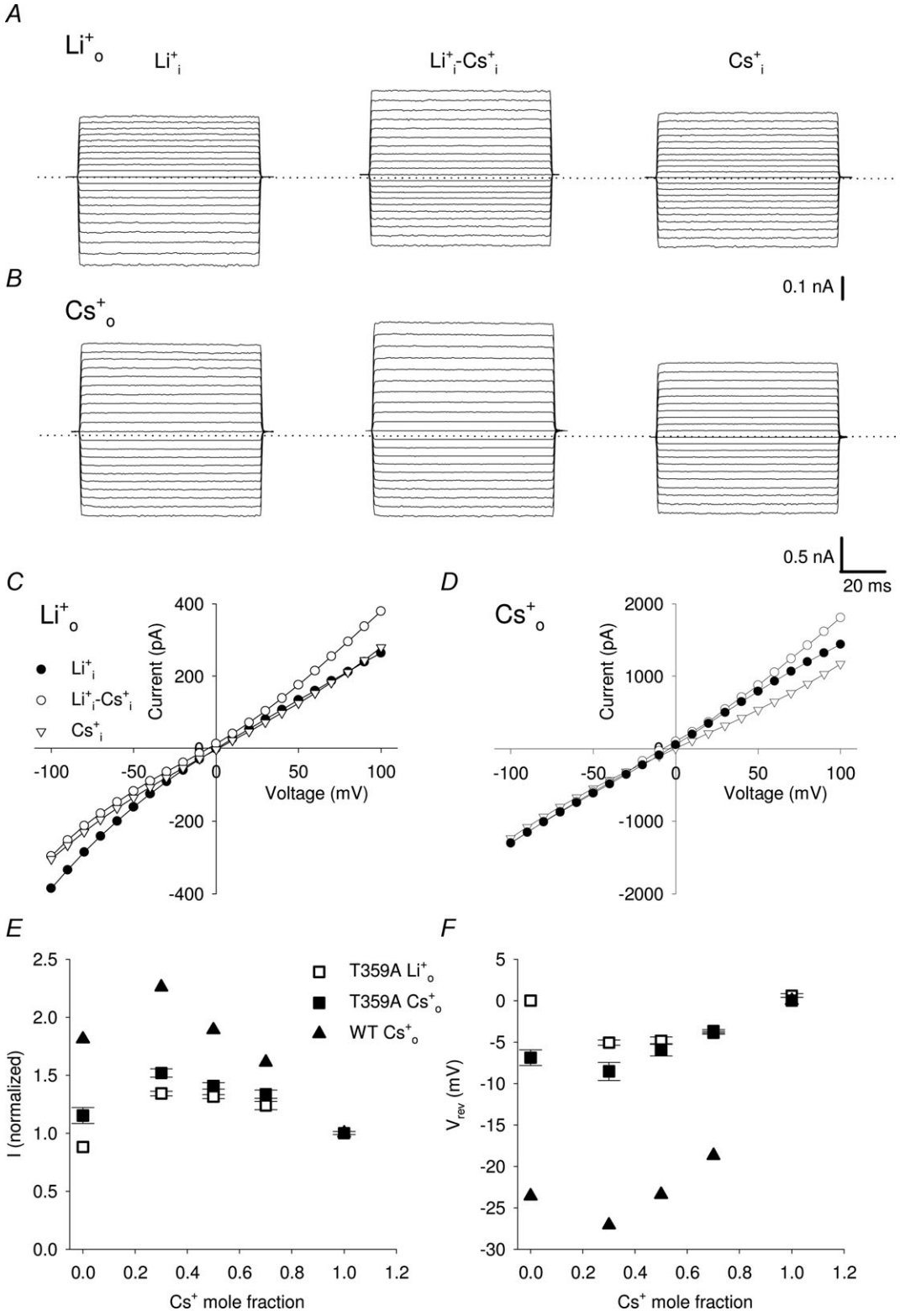

Figure 6. Macroscopic currents through T359A mutant channel in the presence of Li^+ and Cs^+ mixtures and analysis of AMFE

A, representative macroscopic currents through T359A mutant channel from one excised patch in the presence of 110 mM Li^+ inside the patch pipette and different mole fraction of Cs^+ (X_{Cs}) in the bathing solution (being X_{Cs} equal to 0, 0.3 and 1 from left to right). Currents were elicited in the presence of 1 mM cGMP in the bathing medium and voltage steps ranging from −100 to +100 mV (ΔV = 10 mV). Dashed line indicates 0 current level.

AMFE in T359A and T360A mutant channels

Since AMFE has been previously reported in the presence of mixtures of Cs^+ and Li^+ ions in native and WT CNGA1 channels, we investigated this effect in mutant channels T359A and T360A. Figure 6 illustrates current recordings obtained in mutant channel T359A in the presence of either 110 mM Li^+ (Fig. 6*A*) or 110 mM Cs^+ (Fig. 6*B*) in the patch pipette while Li^+ and Cs^+ mixtures are present in the bathing medium. Large macroscopic currents were recorded both in the presence of 100% Li^+ and Cs^+ either when the pipette was filled with 110 mM Li^+ or Cs^+ (Fig. 6*A* and *B*), confirming that both cations are highly permeant. The current flowing in the presence of the Li^+ and Cs^+ mixture, however, was clearly larger than the current flowing either with Cs^+ or Li^+ alone (Fig. 6*A* and *B*). The *I–V* relations obtained in the presence of either 110 mM Cs^+ or 110 mM Li^+ in the patch pipette (Fig 6*C* and *D*) showed that in both cases, the current carried by Li^+–Cs^+ mixtures was larger than the current observed in the presence of either Li^+ or Cs^+ for all voltages more positive than 50 mV. When the Cs^+ mole fraction was 0.3, the outward current was 1.3–1.5 times larger than the current observed in the presence of 100% Cs^+ or Li^+. Figure 6*E* and *F* illustrate several features of the AMFE under various conditions for WT and T359A mutant channels. The normalized current measured at +100 mV shows a peak at $X_{Cs} = 0.3$ both for WT and T359A mutant channels (Fig. 6*E*). The AMFE was also observed measuring V_{rev} (Fig. 6*F*), when the patch pipette was filled either with Li^+ (open squares) or Cs^+ (filled squares).

Also in T360A mutant channels large macroscopic currents were recorded both in the presence of 100% Li^+ and Cs^+ when the pipette was filled with 110 mM of either Li^+ or Cs^+ (Fig. 7*A* and *B*). In contrast to T359A mutant channels, no obvious AMFE was observed when the patch pipette was filled with 110 mM Li^+ (Fig. 7*A* and *C*). The normalized current (Fig. 7*E*) and V_{rev} (Fig. 7*F*) have always an intermediate amplitude between that measured either with 110 mM Cs^+ or Li^+ for all tested Cs^+–Li^+ mixtures. The AMFE in T360A mutant channels was reduced compared to that observed in T359A mutant channels when the patch pipette was filled with 110 mM Cs^+ (Fig. 7*B* and *D*). Normalized currents and V_{rev} show respectively a peak and a drop in the presence of 33 mM Cs^+ and 77 mM Li^+ ($X_{Cs} = 0.3$) as observed in T359A mutant channels (Fig. 7*E* and *F*).

These observations are in agreement with the notion that the hydroxyl group of the Thr360 side chain forms a Cs^+ binding site at the intracellular mouth of the selectivity filter which in concert with the binding site composed by the Glu363 ring determines the AMFE.

Thr359 and Thr360 control selectivity and permeability to monovalent cations

In WT CNGA1 channels, the amplitude of i_{sc} at +140 mV for monovalent cations has been determined to be Na:K:Li:Rb = 1.0:0.8:0.3:0.15 (Nizzari *et al.* 1993). At +140 mV i_{sc} carried by Cs^+ could not be distinguished from the baseline noise. The ionic selectivity in T359A and T360A mutant channels was analysed by substituting the Na^+ present in the medium bathing the cytoplasmic side with other monovalent cations, and by measuring single channel currents at very positive membrane potentials. Figure 8 illustrates single channel recordings from mutant channels T359A and T360A at +100 mV in the presence of Na^+ in the patch pipette and when Na^+ in the bathing solution was replaced with Li^+, K^+, Rb^+ and Cs^+. Discrete open-to-closed transitions were observed for both mutant channels in the presence of all alkali monovalent cations (Fig. 8*A* and *C*). Analysis of the amplitude histograms shows that the i_{sc} for Li^+, Na^+, K^+, Rb^+ and Cs^+ was 0.61, 2.27, 3.71, 3.21 and 0.54 pA for T359A and 0.77, 2.44, 2.93, 2.04 and 1.18 pA for T360A, respectively (Fig. 8*B* and *D*). Hence, the ratio of single channel currents recorded at +100 mV in T359A and T360A mutant channels, respectively, for monovalent cations was:

$$K : Rb : Na : Li : Cs = 1.6 : 1.4 : 1.0 : 0.3 : 0.24$$

and

$$K : Na : Rb : Cs : Li = 1.2 : 1.0 : 0.8 : 0.5 : 0.32$$

This indicates that these mutant channels conduct Rb^+ and Cs^+ significantly more than WT CNGA1 channels do. Measurements of relative ionic permeabilities, obtained from the analysis of V_{rev} under bi-ionic conditions, show that mutant channels T359A and T360A are significantly

B, as in *A*, but with 110 mM Cs^+ inside the patch pipette. *C*, *I–V* curves in T359A mutant channels in the presence of 110 mM Li^+ inside the patch pipette and 110 mM Li^+ (X_{Cs} = 0; filled circles), 33 mM Cs^+ and 77 mM Li^+ (X_{Cs} = 0.3; open circles) and 110 mM Cs^+ (X_{Cs} = 1; open triangles) in the bathing solution. *D*, as in *C*, but with 110 mM Cs^+ inside the patch pipette. *E*, normalized current amplitude flowing at +100 mV in the presence of different Li^+ and Cs^+ mixtures in the bathing solution (being X_{Cs} equal to 0, 0.3, 0.5, 0.7 and 1, respectively) and 110 mM Li^+ (open symbols; n = 5) and 110 mM Cs^+ (filled symbols; n = 4) in the patch pipette for T359A mutant channel (squares) and WT (triangles; redrawn from Sesti *et al.* 1995). Currents were normalized to the current flowing in the absence of Li^+. *F*, dependence of the reversal potential V_{rev} on the Cs^+ mole fraction X_{Cs} in the bathing solution for T359A mutant channels and WT. Solutions and symbols are as described in *E*. Each point was obtained from at least 4 patches.

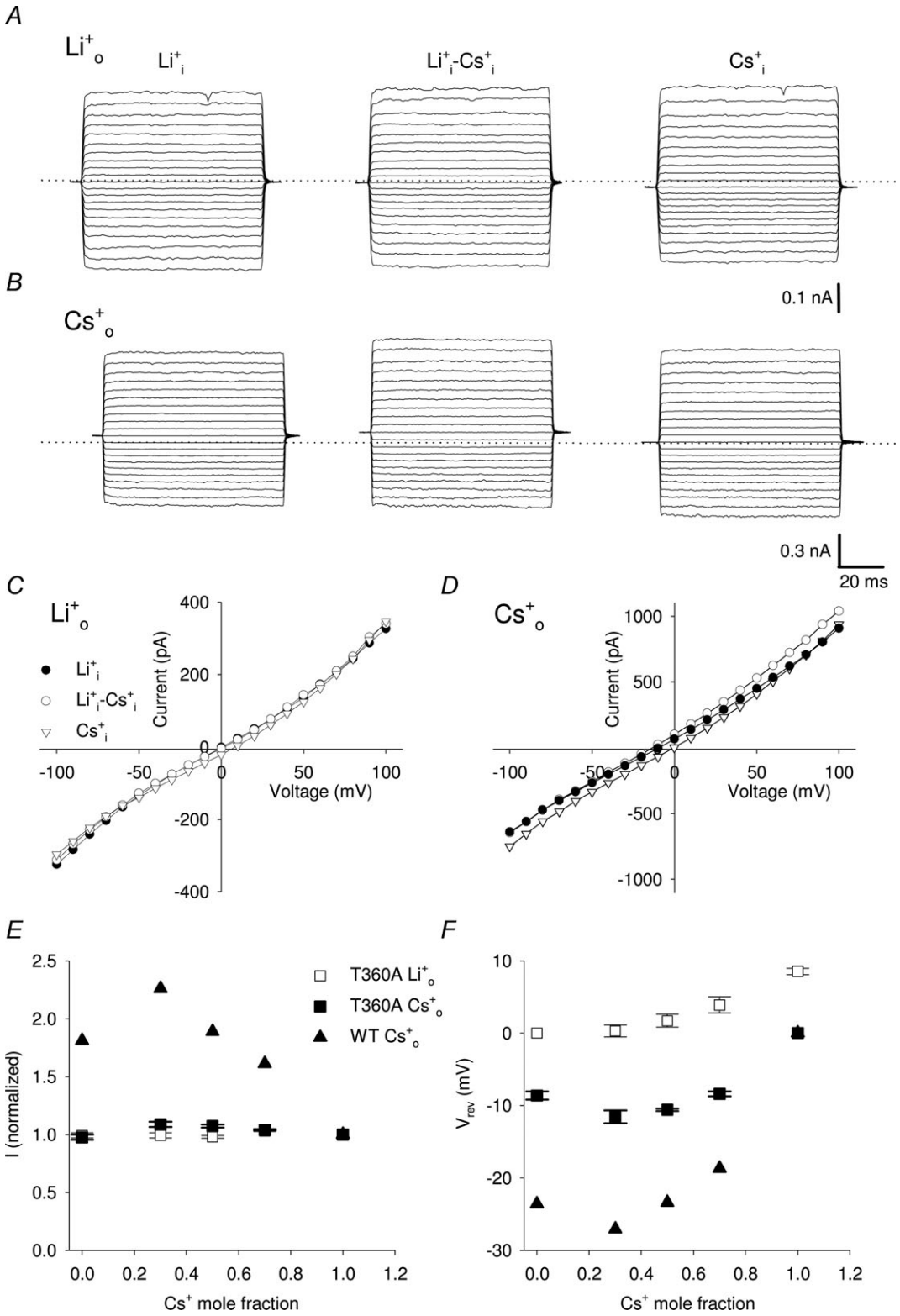

Figure 7. Macroscopic currents through T360A mutant channel in the presence of Li^+ and Cs^+ mixtures
A, representative macroscopic currents through T360A mutant channel from one excised-patch in the presence of 110 mM Li^+ inside the patch pipette and different mole fraction of Cs^+ (X_{Cs}) in the bathing solution (being X_{Cs} equal to 0, 0.3 and 1 from left to right). Recording conditions were as described in Fig. 6. Dashed line indicates 0 current level. *B*, as in *A*, but with 110 mM Cs^+ inside the patch pipette. *C*, *I–V* curves in T360A mutant channels in the presence of 110 mM Li^+ inside the patch pipette and 110 mM Li^+ (X_{Cs} = 0; filled circles), 33 mM Cs^+ and

77 mM Li^+ ($X_{Cs} = 0.3$; open circles) and 110 mM Cs^+ ($X_{Cs} = 1$; open triangles) in the bathing solution. *D*, as in *C*, but with 110 mM Cs^+ inside the patch pipette. *E*, normalized current amplitude flowing at +100 mV in the presence of different Li^+ and Cs^+ mixtures in the bathing solution (being X_{Cs} equal to 0, 0.3, 0.5, 0.7 and 1, respectively) and 110 mM Li^+ (open symbols; $n = 4$) and 110 mM Cs^+ (filles symbols; $n = 4$) in the patch pipette for T360A mutant channel (squares) and WT (triangles; redrawn from Sesti *et al.* 1995). Currents were normalized to the current flowing in the absence of Li^+. *F*, dependence of the reversal potential V_{rev} on the Cs^+ mole fraction X_{Cs} in the bathing solution for T360A mutant channels and WT. Solutions and symbols are as described in *E*. Each point was obtained from at least 4 patches.

more permeable to Cs^+ ions compared to WT CNGA1 channels, with P_{Cs}/P_{Na} equal to 0.97, 0.62 and 0.37 for T359A, T360A and WT, respectively (Table 1).

Discussion

Previous studies have shown that CNG channels are multi-ion pores and that the ring of Glu363 near the extracellular vestibule of the pore constitutes a major binding site for divalent and monovalent cations as well as for protons (Furman & Tanaka, 1990; Root & MacKinnon, 1993, 1994; Eismann *et al.* 1994; Sesti *et al.* 1995; Rho & Park, 1998; Qu *et al.* 2001). The present paper shows that the ring of Thr360 at the intracellular vestibule forms another ion binding site, controlling monovalent cation selectivity and permeation. We discuss here more in detail the properties of the binding site composed by the ring of Thr360 and how the pore structure of CNG channels determines its selectivity and permeation.

Origin of the inward Na^+ current inhibition by Rb^+ and Cs^+

When Rb^+ and Cs^+ ions are present in the internal cavity, Na^+ inward current is reduced and this blockage is stronger in the presence of Cs^+ and is relieved at negative voltages (Fig. 2). The voltage dependency of the Rb^+/Cs^+ blockage argues against any simple intracellular modulatory-site mechanism since it is not expected to be voltage dependent (Plested, 2011). Moreover, analysis of single channel current fluctuations shows that Cs^+ inhibition is due to both a lower amplitude of the single channel current and to the appearance of longer closed states (Fig. 3). Neutralization of Thr360 in the intracellular vestibule almost completely abolishes this blockage suggesting that Rb^+ and Cs^+ could interact directly and/or indirectly through a water molecule with the hydroxyl group of Thr360. In this view, voltage dependency of the blockage arises from the binding of these ions within the electrical field focused on the selectivity filter (Contreras *et al.* 2010).

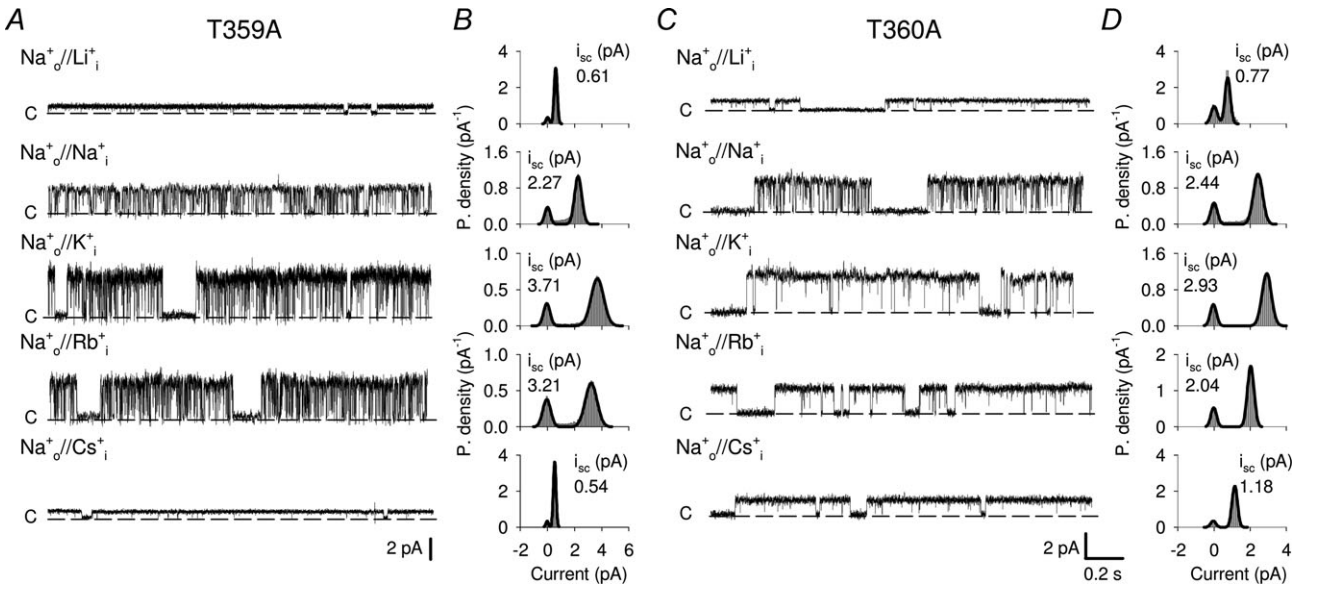

Figure 8. Single channel ionic selectivity in T359A and T360A mutant channels
A, current recordings from one T359A mutant channel at +100 mV in the presence of 110 mM Na^+ in the patch pipette and 110 mM Li^+, Na^+, K^+, Rb^+ and Cs^+ in the bathing medium. Dashed lines indicate the closed state. Currents were elicited in the presence of 1 mM cGMP. *B*, all-point amplitude histograms from recordings in *A*. The continuous line represents a two component Gaussian fit. i_{sc} indicates the single channel current amplitude. *C*, as in *A*, but for T360A mutant channel. *D*, as in *B*, but for T360A mutant channel.

Table 1. Permeability ratios (P_X/P_{Na}) of WT CNGA1 and of T359A and T360A mutant channels

	Li^+		K^+		Rb^+		Cs^+	
Mutant	V_{rev} (mV)	P_{Li}/P_{Na}	V_{rev} (mV)	P_K/P_{Na}	V_{rev} (mV)	P_{Rb}/P_{Na}	V_{rev} (mV)	P_{Cs}/P_{Na}
WT	8.9 ± 1.2	0.71	1.45 ± 0.6	0.95	8.6 ± 1.0	0.72	26.6 ± 1.8	0.36
T359A	20.1 ± 3.3	0.45	−8.3 ± 0.7	1.37	−4.7 ± 3.2	1.20	0.7 ± 4.2	0.97
T360A	9.5 ± 2.5	0.69	−1.4 ± 2.0	1.05	6.5 ± 3.0	0.78	12.5 ± 3.0	0.62

In the crystal structure of CNG-mimicking chimeras the side chains of Thr62, equivalent to Thr359 in WT CNGA1 channels, point away from the permeation pathway seemingly unable to make direct contact with permeating ions. Indeed, Thr62 side chains interact with neighbour residues in the selectivity filter stabilizing the pore architecture. Therefore, neutralization of Thr359 is expected to alter the conformation of the intracellular mouth of the selectivity filter that is likely to modify Cs^+ and Rb^+ coordination to Thr360.

Interestingly, similar mechanisms of blockage have been observed in the KcsA channel when Li^+ or Na^+ ions are present in the cavity blocking K^+ current (Nimigean & Miller, 2002; Thompson *et al.* 2009). In these studies both, a fast and a slow blockage have been observed and were associated respectively to a low affinity binding site in the internal cavity and to a higher affinity binding site within the selectivity filter, near the plane of Thr75 carbonyl atoms, as confirmed also by molecular dynamics (MD) simulations and crystallographic data. Albeit Cs^+ blockage in CNGA1 could reflect similar mechanisms, an alternative intriguing explanation could be that Cs^+ ions bind to the conductive and non-conductive configurations of the selectivity filter resulting in different mechanisms of blockage. Indeed the primary gate in CNG channels has been located within the selectivity filter itself (Fodor *et al.* 1997; Becchetti & Roncaglia, 2000; Contreras *et al.* 2008) and this hypothesis is consistent with previously reported state-dependent reactivity of cystein mutants in position 360 using transition metal ions as probes (Becchetti & Roncaglia, 2000).

The role of Thr359 and Thr360 in ion conduction, selectivity and permeation

The presence of AMFE in rod and olfactory CNG channels has been previously observed and according to the most-accepted mechanisms underlying it, AMFE has been associated to an interaction between ions in the channel pore indicating the multiple-ion occupancy of the channel (Hagiwara *et al.* 1977; Hille & Schwarz, 1978; Hille, 1992). Moreover Sesti *et al.* (1995) suggested that the molecular basis for multi-ion interactions in CNGA1 channels involved the glutamate 363, constituting a major binding site within the pore. We have found that mutation of Thr359 does not affect AMFE significantly compared to WT channels. Indeed the normalized current at +100 mV in both channels has a maximum at $X_{Cs} = 0.3$ when either Li^+ or Cs^+ were present in the patch pipette (Fig. 6). V_{rev} in these solutions also demonstrated AMFE, further supporting the multi-ion nature of these channels, since V_{rev} does not depend on the number of open channels (Fig 6). These observations are consistent with the crystal structures of CNG mimicking chimeras, where only Thr360 interacts with permeating ions and Thr359 does not contribute directly to ion binding within the selectivity filter. In T360A mutant channels AMFE was abolished when Li^+ ions were present in the patch pipette (Fig. 7). However, AMFE could be still detected in V_{rev} if the patch pipette was filled with 110 mM Cs^+, signalling the presence of two ions within the pore (Fig. 7). Crystallographic data and MD simulations have shown that smaller Na^+ and Li^+ ions do not coordinate at the centre of the carbonyls cage in the selectivity filter like larger K^+ and Rb^+, but tend to binds in a plane with carbonyl oxygens (Thompson *et al.* 2009; Ye *et al.* 2010; Derebe *et al.* 2011*b*). In this view, it is possible to imagine the simultaneous presence of two differently sized ions in the selectivity filter of the T360A mutant channel; a larger ion like Cs^+ could bind 'in cage' at site S_2 and a smaller ion like Li^+ could be coordinated in-plane by backbone carbonyls of Ala360, separated by a water molecule. The fact that AMFE was observed only when Cs^+ ions were present in the patch pipette but not Li^+ ions is likely to reflect the architectural asymmetries of the extracellular and intracellular mouth of the selectivity filter.

In WT CNGA1 channel both Rb^+ and Cs^+ are less permeant than Na^+ ions. The single channel conductance at +100 mV for Na^+ is around 30 pS while it is only 5 pS in Rb^+ (Kusch *et al.* 2004) and it could not be determined in Cs^+ at membrane potentials up to +140 mV (Nizzari *et al.* 1993). We propose that the Thr360 hydroxyl group contributes to this ion binding site, stabilizing Rb^+ and Cs^+ in the S_4 position and reducing their permeation. In fact replacement of Thr359 or Thr360 with an alanine significantly increases Rb^+ and Cs^+ permeabilities and well-resolved openings could be detected at +100 mV

when Cs^+ ions were present in the bathing medium (Fig. 7 and Table 1). Mutation of Thr359 is likely to result in a local perturbation of the intracellular mouth of the selectivity filter affecting Thr360 side chain orientation and hence monovalent cation conduction, permeation and selectivity.

Similarities and differences in the pore of CNG and K^+ channels

Our electrophysiological results and the molecular structure of the pore of the CNG mimics (Derebe *et al.* 2011*b*) reveal one major similarity and two fundamental differences between the pore of CNG and K^+ channels.

Crystallographic and electrophysiological data suggest that the intracellular vestibule of CNG and K^+ channels have a similar architecture with two threonines (Fig. 1) playing a very similar role. The threonines closer to the P-helix (Thr359 in CNGA1 channels) have side chains pointing towards the interior of the protein providing structural stability, while the other threonines closer to the narrowest region of the pore (Thr360 in CNGA1 channels) constitute a binding site for cations.

The substitution of the motif GYG – the signature of K^+ channels – with the ETPP motif present in the vast majority of CNG channels removes the first ion binding site (S_1) in the selectivity filter, resulting in major structural differences at the extracellular vestibule. This site is replaced by a concave funnel shaped vestibule with the pyrrolidine ring from Pro68 forming the wall of the funnel (Fig. 1*C*). This proline is conserved among all known CNG channels and is not present in either K^+ or Na^+ channels. Previous electrophysiological investigations have identified this proline as part of the external vestibule (Becchetti *et al.* 1999) and mutant P365T channels have profoundly anomalous permeation and gating (Gamel & Torre, 2000). These observations suggest that the overall architecture at the intracellular mouth of the selectivity filter is rather similar in CNG and K^+ channels but it is not so for the extracellular mouth.

While the selectivity filter of K^+ channels can accommodate up to three ions, not more than two ions can be present at the same time in the pore of CNG channels. This difference, which seems to be well established, is likely to be at the basis of the different selectivity of CNG and K^+ channels. Studies of NaK channels and of its various mutants demonstrate that four contiguous ion-binding sites in the filter are a necessary prerequisite for a selective and efficient K^+ conduction (Derebe *et al.* 2011*a*,*b*). CNG channels with only three binding sites in the filter are poorly selective.

The results of the present study suggest a possible physiological relevance of the ring of threonines in the inner vestibule of the pore of CNG channels. CNG channels were originally detected in photoreceptor and olfactory neurons but they are also present in several non-sensory neurons; there is also extensive evidence for the expression of several CNG channel subtypes in the central nervous system (Zufall *et al.* 1997; Kaupp & Seifert, 2002). Because of their high permeability to Ca^{2+}, CNG channels have the potential to influence numerous cellular functions, including cell excitability and several Ca^{2+}-dependent intracellular processes. The two rings of threonines in the intracellular vestibule are highly conserved in the great majority of K^+ and of CNG channels of both A and B subunits. Therefore, possibly all CNG channels have a binding site for cations near their intracellular vestibule which could play a regulatory role in CNG channels in different tissues, in particular in CNS (Zufall *et al.* 1997; Podda *et al.* 2008; Togashi *et al.* 2008; Lopez-Jimenez *et al.* 2012). For instance, CNG channels are involved in growth cone pathfinding and the intracellular ring of threonines here described could be part of the orchestration of growth cone attraction and repulsion (Togashi *et al.* 2008; Lopez-Jimenez *et al.* 2012). Indeed it has been established that CNG channels are modulated by different intracellular molecules like diacylglicerol, retinoids and polyamines possibly involving interactions with polar groups within the channel pore (Lu & Ding, 1999; Crary *et al.* 2000; Horrigan *et al.* 2005). Moreover the ring of Thr360 could be or could contribute to the receptor site for many voltage-dependent intracellular CNG channels blockers, like dequalinium, L-cis-diltiazem and tetracaine (Brown *et al.* 2006). The two binding sites composed of the rings of Glu363 and Thr360 are not independent, so divalent cations permeation and blockage may be attributable to the multi-ion occupancy of the channel.

References

Anselmi C, Carloni P & Torre V (2007). Origin of functional diversity among tetrameric voltage-gated channels. *Proteins* **66**, 136–146.

Becchetti A, Gamel K & Torre V (1999). Cyclic nucleotide-gated channels. Pore topology studied through the accessibility of reporter cysteines. *J Gen Physiol* **114**, 377–392.

Becchetti A & Roncaglia P (2000). Cyclic nucleotide-gated channels: intra- and extracellular accessibility to Cd^{2+} of substituted cysteine residues within the P-loop. *Pflugers Arch* **440**, 556–565.

Bernèche S & Roux B (2001). Energetics of ion conduction through the K^+ channel. *Nature* **414**, 73–77.

Bernèche S & Roux B (2003). A microscopic view of ion conduction through the K^+ channel. *Proc Natl Acad Sci U S A* **100**, 8644–8648.

Biel M & Michalakis S (2009). Cyclic nucleotide-gated channels. In *Handbook of Experimental Pharmacology*, vol. 191, *cGMP: Generators, Effectors and Therapeutic Implications*, ed. Schmidt HHHW, Hofmann F & Stasch J-P, pp. 111–136. Springer, Berlin, Heidelberg.

Biel M, Zong X, Ludwig A, Sautter A & Hofmann F (1999). Structure and function of cyclic nucleotide-gated channels. *Rev Physiol Biochem Pharmacol* **135**, 151–171.

Brohawn SG, del Mármol J & MacKinnon R (2012). Crystal structure of the human K2P TRAAK, a lipid- and mechano-sensitive K^+ ion channel. *Science* **335**, 436–441.

Brown RL, Strassmaier T, Brady JD & Karpen JW (2006). The Pharmacology of cyclic nucleotide-gated channels: emerging from the darkness. *Curr Pharm Des* **12**, 3597–3613.

Bucossi G, Nizzari M & Torre V (1997). Single-channel properties of ionic channels gated by cyclic nucleotides. *Biophys J* **72**, 1165–1181.

Contreras JE, Chen J, Lau AY, Jogini V, Roux B & Holmgren M (2010). Voltage profile along the permeation pathway of an open channel. *Biophys J* **99**, 2863–2869.

Contreras JE & Holmgren M (2006). Access of quaternary ammonium blockers to the internal pore of cyclic nucleotide-gated channels: implications for the location of the gate. *J Gen Physiol* **127**, 481–494.

Contreras JE, Srikumar D & Holmgren M (2008). Gating at the selectivity filter in cyclic nucleotide-gated channels. *Proc Natl Acad Sci U S A* **105**, 3310–3314.

Crary JI, Dean DM, Nguitragool W, Kurshan PT & Zimmerman AL (2000). Mechanism of inhibition of cyclic nucleotide-gated ion channels by diacylglycerol. *J Gen Physiol* **116**, 755–768.

Craven KB & Zagotta WN (2006). CNG and HCN channels: two peas, one pod. *Annu Rev Physiol* **68**, 375–401.

Derebe MG, Sauer DB, Zeng W, Alam A, Shi N & Jiang Y (2011*a*). Tuning the ion selectivity of tetrameric cation channels by changing the number of ion binding sites. *Proc Natl Acad Sci U S A* **108**, 598–602.

Derebe MG, Zeng W, Li Y, Alam A & Jiang Y (2011*b*). Structural studies of ion permeation and Ca^{2+} blockage of a bacterial channel mimicking the cyclic nucleotide-gated channel pore. *Proc Natl Acad Sci U S A* **108**, 592–597.

Doyle DA, Morais Cabral J, Pfuetzner RA, Kuo A, Gulbis JM, Cohen SL, Chait BT & MacKinnon R (1998). The structure of the potassium channel: molecular basis of K^+ conduction and selectivity. *Science* **280**, 69–77.

Eismann E, Müller F, Heinemann SH & Kaupp UB (1994). A single negative charge within the pore region of a cGMP-gated channel controls rectification, Ca^{2+} blockage, and ionic selectivity. *Proc Natl Acad Sci U S A* **91**, 1109–1113.

Flynn GE & Zagotta WN (2001). Conformational changes in S6 coupled to the opening of cyclic nucleotide-gated channels. *Neuron* **30**, 689–698.

Flynn GE & Zagotta WN (2003). A cysteine scan of the inner vestibule of cyclic nucleotide-gated channels reveals architecture and rearrangement of the pore. *J Gen Physiol* **121**, 563–582.

Fodor AA, Black KD & Zagotta WN (1997). Tetracaine reports a conformational change in the pore of cyclic nucleotide-gated channels. *J Gen Physiol* **110**, 591–600.

Furman RE & Tanaka JC (1990). Monovalent selectivity of the cyclic guanosine monophosphate-activated ion channel. *J Gen Physiol* **96**, 57–82.

Gamel K & Torre V (2000). The interaction of Na^+ and K^+ in the pore of cyclic nucleotide-gated channels. *Biophys J* **79**, 2475–2493.

Giorgetti A, Nair AV, Codega P, Torre V & Carloni P (2005). Structural basis of gating of CNG channels. *FEBS Lett* **579**, 1968–1972.

Guex N & Peitsch MC (1997). SWISS-MODEL and the Swiss-PdbViewer: an environment for comparative protein modeling. *Electrophoresis* **18**, 2714–2723.

Hagiwara S, Miyazaki S, Krasne S & Ciani S (1977). Anomalous permeabilities of the egg cell membrane of a starfish in K^+-Tl^+ mixtures. *J Gen Physiol* **70**, 269–281.

Hamill OP, Marty A, Neher E, Sakmann B & Sigworth FJ (1981). Improved patch-clamp techniques for high-resolution current recording from cells and cell-free membrane patches. *Pflugers Arch* **391**, 85–100.

Heginbotham L, Abramson T & MacKinnon R (1992). A functional connection between the pores of distantly related ion channels as revealed by mutant K^+ channels. *Science* **258**, 1152–1155.

Heginbotham L, Lu Z, Abramson T & MacKinnon R (1994). Mutations in the K^+ channel signature sequence. *Biophys J* **66**, 1061–1067.

Higgins MK, Weitz D, Warne T, Schertler GFX & Kaupp UB (2002). Molecular architecture of a retinal cGMP-gated channel: the arrangement of the cytoplasmic domains. *EMBO J* **21**, 2087–2094.

Hille B (1992). *Ionic Channels of Excitable Membranes*, 2nd edn, Sinauer Associates Inc., Sunderland, MA.

Hille B & Schwarz W (1978). Potassium channels as multi-ion single-file pores. *J Gen Physiol* **72**, 409–442.

Hodgkin AL & Keynes RD (1955). The potassium permeability of a giant nerve fibre. *J Physiol* **128**, 61–88.

Horrigan DM, Tetreault ML, Tsomaia N, Vasileiou C, Borhan B, Mierke DF, Crouch RK & Zimmerman AL (2005). Defining the retinoid binding site in the rod cyclic nucleotide-gated channel. *J Gen Physiol* **126**, 453–460.

Jan LY & Jan YN (1990). A superfamily of ion channels. *Nature* **345**, 672.

Jan LY & Jan YN (1992). Tracing the roots of ion channels. *Cell* **69**, 715–718.

Jiang Y, Lee A, Chen J, Cadene M, Chait BT & MacKinnon R (2002). The open pore conformation of potassium channels. *Nature* **417**, 523–526.

Jiang Y, Lee A, Chen J, Ruta V, Cadene M, Chait BT & MacKinnon R (2003). X-ray structure of a voltage-dependent K^+ channel. *Nature* **423**, 33–41.

Kaupp UB, Niidome T, Tanabe T, Terada S, Bönigk W, Stühmer W, Cook NJ, Kangawa K, Matsuo H & Hirose T (1989). Primary structure and functional expression from complementary DNA of the rod photoreceptor cyclic GMP-gated channel. *Nature* **342**, 762–766.

Kaupp UB & Seifert R (2002). Cyclic nucleotide-gated ion channels. *Physiol Rev* **82**, 769–824.

Kusch J, Nache V & Benndorf K (2004). Effects of permeating ions and cGMP on gating and conductance of rod-type cyclic nucleotide-gated (CNGA1) channels. *J Physiol* **560**, 605–616.

Liu J & Siegelbaum SA (2000). Change of pore helix conformational state upon opening of cyclic nucleotide-gated channels. *Neuron* **28**, 899–909.

Long SB, Campbell EB & Mackinnon R (2005). Crystal structure of a mammalian voltage-dependent Shaker family K^+ channel. *Science* **309**, 897–903.

Lopez-Jimenez ME, González JC, Lizasoain I, Sánchez-Prieto J, Hernández-Guijo JM & Torres M (2012). Functional cGMP-gated channels in cerebellar granule cells. *J Cell Physiol* **227**, 2252–2263.

Lu Z & Ding L (1999). Blockade of a retinal cGMP-gated channel by polyamines. *J Gen Physiol* **113**, 35–43.

Mazzolini M, Anselmi C & Torre V (2009). The analysis of desensitizing CNGA1 channels reveals molecular interactions essential for normal gating. *J Gen Physiol* **133**, 375–386.

Mazzolini M, Marchesi A, Giorgetti A & Torre V (2010). Gating in CNGA1 channels. *Pflugers Arch* **459**, 547–555.

Menini A (1990). Currents carried by monovalent cations through cyclic GMP-activated channels in excised patches from salamander rods. *J Physiol* **424**, 167–185.

Menini A (1995). Cyclic nucleotide-gated channels in visual and olfactory transduction. *Biophys Chem* **55**, 185–196.

Morais-Cabral JH, Zhou Y & MacKinnon R (2001). Energetic optimization of ion conduction rate by the K^+ selectivity filter. *Nature* **414**, 37–42.

Nair AV, Nguyen CHH & Mazzolini M (2009). Conformational rearrangements in the S6 domain and C-linker during gating in CNGA1 channels. *Eur Biophys J* **38**, 993–1002.

Nimigean CM & Miller C (2002). Na^+ block and permeation in a K^+ channel of known structure. *J Gen Physiol* **120**, 323–335.

Nizzari M, Sesti F, Giraudo MT, Virginio C, Cattaneo A & Torre V (1993). Single-channel properties of cloned cGMP-activated channels from retinal rods. *Proc Biol Sci* **254**, 69–74.

Picco C & Menini A (1993). The permeability of the cGMP-activated channel to organic cations in retinal rods of the tiger salamander. *J Physiol* **460**, 741–758.

Plested AJR (2011). Kainate receptor modulation by sodium and chloride. *Adv Exp Med Biol* **717**, 93–113.

Podda MV, D'Ascenzo M, Leone L, Piacentini R, Azzena GB & Grassi C (2008). Functional role of cyclic nucleotide-gated channels in rat medial vestibular nucleus neurons. *J Physiol* **586**, 803–815.

Qu W, Moorhouse AJ, Cunningham AM & Barry PH (2001). Anomalous mole-fraction effects in recombinant and native cyclic nucleotide-gated channels in rat olfactory receptor neurons. *Proc Biol Sci* **268**, 1395–1403.

Rho SH & Park CS (1998). Extracellular proton alters the divalent cation binding affinity in a cyclic nucleotide-gated channel pore. *FEBS Lett* **440**, 199–202.

Root MJ & MacKinnon R (1993). Identification of an external divalent cation-binding site in the pore of a cGMP-activated channel. *Neuron* **11**, 459–466.

Root MJ & MacKinnon R (1994). Two identical noninteracting sites in an ion channel revealed by proton transfer. *Science* **265**, 1852–1856.

Sesti F, Eismann E, Kaupp UB, Nizzari M & Torre V (1995). The multi-ion nature of the cGMP-gated channel from vertebrate rods. *J Physiol* **487**, 17–36.

Stryer L (1986). Cyclic GMP cascade of vision. *Annu Rev Neurosci* **9**, 87–119.

Tao X, Avalos JL, Chen J & MacKinnon R (2009). Crystal structure of the eukaryotic strong inward-rectifier K^+ channel Kir2.2 at 3.1 Å resolution. *Science* **326**, 1668–1674.

Tetreault ML, Henry D, Horrigan DM, Matthews G & Zimmerman AL (2006). Characterization of a novel cyclic nucleotide-gated channel from zebrafish brain. *Biochem Biophys Res Commun* **348**, 441–449.

Thompson AN, Kim I, Panosian TD, Iverson TM, Allen TW & Nimigean CM (2009). Mechanism of potassium-channel selectivity revealed by Na^+ and Li^+ binding sites within the KcsA pore. *Nat Struct Mol Biol* **16**, 1317–1324.

Togashi K, von Schimmelmann MJ, Nishiyama M, Lim C-S, Yoshida N, Yun B, Molday RS, Goshima Y & Hong K (2008). Cyclic GMP-gated CNG channels function in Sema3A-induced growth cone repulsion. *Neuron* **58**, 694–707.

Ye S, Li Y & Jiang Y (2010). Novel insights into K^+ selectivity from high-resolution structures of an open K^+ channel pore. *Nat Struct Mol Biol* **17**, 1019–1023.

Yu FH, Yarov-Yarovoy V, Gutman GA & Catterall WA (2005). Overview of molecular relationships in the voltage-gated ion channel superfamily. *Pharmacol Rev* **57**, 387–395.

Zagotta WN (2006). Membrane biology: permutations of permeability. *Nature* **440**, 427–429.

Zhou Y, Morais-Cabral JH, Kaufman A & MacKinnon R (2001). Chemistry of ion coordination and hydration revealed by a K^+ channel-Fab complex at 2.0 Å resolution. *Nature* **414**, 43–48.

Zimmerman AL (1995). Cyclic nucleotide gated channels. *Curr Opin Neurobiol* **5**, 296–303.

Zufall F, Shepherd GM & Barnstable CJ (1997). Cyclic nucleotide gated channels as regulators of CNS development and plasticity. *Curr Opin Neurobiol* **7**, 404–412.

Author contributions

A.M. performed experiments on oocytes; M.M. performed mutagenesis; A.M., M.M and V.T. participated in designing experiments, analysing, interpreting data and contributed to writing the paper; V.T. supervised the project. All authors approved the final version of the manuscript.

Acknowledgements

We thank M. Lough for checking the English. This work was supported by a COFIN grant from the Italian Ministry, SMD Contract no. 229375 (FP7-NMP-2008-SMALL-1) from the EU and FOCUS Contract no. 270483 (FP7-ICT-2009-6) from the EU.